Society of Medical Education & Research

2024, Volume 4, Issue 2, Page No: 45-65
ISSN: 3108-4834

Archive of International Journal of Cancer and Allied Science

eNAMPT Blockade Disrupts PD-L1/PD-1 Axis to Counter T-Cell Evasion in Breast Cancer

Anke Maria Fischer[1]*, Johannes Lukas Weber[1]

[1]Department of Hematology and Oncology, University of Heidelberg, Heidelberg, Germany.

***E-mail** ✉ a.fischer.uni-hd@yahoo.com

Abstract

Nicotinamide phosphoribosyltransferase (NAMPT) plays a pivotal intracellular role in maintaining nicotinamide adenine dinucleotide (NAD) metabolism, but it is also secreted into the extracellular space, where it functions as a cytokine (eNAMPT). Elevated circulating eNAMPT levels have been reported in inflammatory disorders and malignant diseases. In breast cancer patients, plasma eNAMPT concentrations are increased and show a strong association with disease stage and patient prognosis. On this basis, we explored the involvement of eNAMPT in the progression of triple-negative mammary tumors by assessing the impact of its inhibition using a specific neutralizing monoclonal antibody (C269). Female BALB/c mice were inoculated with 4T1 clone 5 cells, while female C57BL6 mice received EO771 cells. Tumor growth, spleen enlargement and metastatic dissemination were monitored. The anti-eNAMPT neutralizing antibody was administered twice weekly, and animals were sacrificed after 28 days. Excised tumors were examined using histopathological techniques, flow cytometry, western blotting, immunohistochemistry, immunofluorescence and RNA sequencing. These analyses enabled detailed characterization of tumor properties, including the isolation of tumor-infiltrating lymphocytes and cancer cells, and allowed investigation of the molecular pathways responsible for the observed effects. Additionally, three-dimensional (3D) co-culture systems were employed to analyze functional interactions between tumor cells and T lymphocytes. Treatment with C269-mediated eNAMPT blockade significantly reduced primary tumor burden and lowered the incidence of lung metastases. Transcriptomic profiling combined with functional experiments demonstrated that eNAMPT modulated T-cell activity through the programmed death-ligand 1/programmed cell death protein 1 (PD-L1/PD-1) signaling axis. Neutralization of eNAMPT restored effective antitumor immunity, characterized by enhanced activation of CD8+IFNγ+GrzB+ T cells and a marked attenuation of the immunosuppressive phenotype of regulatory T cells. Together, these findings provide the first evidence that eNAMPT represents a previously unrecognized immunotherapeutic target in triple-negative breast cancer.

Keywords: Breast neoplasms, Cytokines, Immunotherapy, Lymphocyte activation

Introduction

Over the last decade, immunotherapy has dramatically altered the landscape of cancer treatment. Agents targeting cytotoxic T-lymphocyte antigen 4 (CTLA-4) and programmed death-ligand 1/programmed cell death protein 1 (PD-L1/PD-1) have improved outcomes across a wide range of malignancies and disease stages, spanning from adjuvant therapy to advanced disease and from melanoma to lymphomas [1]. In parallel, additional modalities—including bispecific antibodies that physically link tumor cells with immune effector cells [2, 3] and chimeric antigen receptor (CAR) T-cell therapies [4]—have further transformed clinical practice. Both PD-1/PD-L1- and CTLA4-targeted strategies operate by interrupting cellular interactions that permit immune escape [1]. Alternatively, immunotherapy may also be directed toward disrupting the upstream regulatory mechanisms that control the expression of membrane proteins responsible for these immune-suppressive interactions [1].

Access this article online https://smerpub.com/

Received: 17 April 2024; **Accepted:** 26 July 2024

How to cite this article: Fischer AM, Weber JL. eNAMPT Blockade Disrupts PD-L1/PD-1 Axis to Counter T-Cell Evasion in Breast Cancer. Arch Int J Cancer Allied Sci. 2024;4(2):45-65. https://doi.org/10.51847/K6AYtuXGqa

NAMPT is a cytosolic enzyme required for NAD biosynthesis, and its pharmacological inhibition has been shown to impair tumor growth by inducing metabolic stress in malignant cells and by influencing myeloid-derived suppressor cell activity [5]. However, NAMPT can also be actively secreted, where it functions as an extracellular cytokine (eNAMPT) [6–9]. This extracellular form is identical to pre-B cell enhancing factor, initially described for its synergistic effects with interleukin 7 and stem cell factor in expanding pre-B cell colonies [10], and to visfatin, a cytokine released by adipose tissue [11]. Notably, elevated plasma eNAMPT levels have been documented in cancer patients and correlate with clinical outcomes [12, 13]. Although the precise contribution of eNAMPT to tumor biology remains incompletely defined, it is known to influence inflammatory processes and to modulate both innate and adaptive immune responses [14–17]. The molecular mechanisms mediating eNAMPT signaling outside the cell remain only partially understood [16, 18, 19]. A direct interaction with the C-C chemokine receptor type 5 (CCR5) has been proposed by Van den Bergh *et al*. [19], and we subsequently demonstrated that eNAMPT can act as an antagonist of this receptor [20]. While activation of toll-like receptor 4 (TLR4) currently appears to be the dominant signaling mechanism [18, 21], our recent findings indicate that TLR4 does not represent the sole receptor involved [16].

The objective of the present study was to clarify the role of eNAMPT in triple-negative breast cancer (TNBC), a subtype that continues to exhibit the poorest clinical outcome among breast cancers [22]. Elevated eNAMPT concentrations after surgical intervention are associated with reduced disease-free and overall survival [23] and correlate with TNM classification, tumor size, lymph node metastasis and histological grade [24]. To dissect the contribution of this cytokine, we employed a neutralizing antibody that selectively targets the extracellular form of NAMPT without altering intracellular metabolic activity [13, 15]. We demonstrate that eNAMPT regulates the PD-1/PD-L1 immune checkpoint axis in both tumor cells and T lymphocytes, and that antibody-mediated neutralization disrupts PD-1/PD-L1–dependent immune escape. Collectively, these results strongly support eNAMPT as a novel and actionable therapeutic target in TNBC.

Materials and Methods

Syngeneic orthotopic mammary carcinoma mouse model

All animal experiments were performed in accordance with Italian law and received authorization from the Ministry of Health (120/2018 DB064.30 of 27/03/2018). Study reporting followed ARRIVE1 (Animal Research: Reporting of In Vivo Experiments) standards [25]. Female mice aged 8–10 weeks were included in all experimental protocols. BALB/C mice, BALB/c Nude mice (Charles River Laboratories) and C57BL/6 mice (Envigo Laboratories) were housed under standardized environmental conditions consisting of a 12 hour light/dark cycle, temperature maintained at 21±1°C and relative humidity of 50±5%. Animals had continuous access to standard chow and drinking water.

The 4T1 clone 5 cell line [26] was propagated in minimum essential medium (MEM) supplemented with 10% fetal bovine serum (FBS), 2 mmol/L L-glutamine and 10 µg/mL penicillin–streptomycin. EO771 cells (ATCC, CRL-3461) were cultured in Dulbecco's modified Eagle medium (DMEM) containing identical supplements. Orthotopic implantation was performed by injecting 7×10^3 4T1 (or 4T1-GFP) cells into the mammary fat pad of BALB/C mice or 5×10^5 EO771 cells into C57BL/6 mice using a 26-gauge needle.

Treatments were administered intraperitoneally (i.p.) and consisted of vehicle alone (phosphate-buffered saline (PBS), twice weekly), an isotype control antibody (Mouse IgG1 HKSP84, Ichorbio; 2.5 mg/kg in PBS, twice weekly), or the eNAMPT-neutralizing antibody C269 (2.5 mg/kg in PBS, twice weekly). Unless otherwise specified, C269 treatment commenced on day 1 after tumor implantation (eg, immunophenotyping, RNA sequencing (RNAseq)). In selected therapeutic experiments, treatment initiation was delayed until day 15 following randomization based on tumor volume. The humanized monoclonal antibody targeting eNAMPT, ALT-200 (Aqualung Therapeutics), was administered i.p. at 0.4 mg/kg every 7 days. Anti–PD-1 (InVivoMab, Bio X Cell, clone RMP1-14) and anti–PD-L1 (InVivoPlus, Bio X Cell, clone 10F.9G2) antibodies were delivered i.p. at 2 mg/kg on days 4, 8 and 12.

Tumor size was measured with calipers starting on day 15. On day 28, animals were euthanized, blood samples collected, and spleens, primary tumors and lungs excised. Tumor and spleen masses were recorded, lungs were rinsed with PBS, and metastatic lesions were quantified.

Metastasis evaluation

Clonogenic assay

Excised lungs were finely dissected and enzymatically digested using collagenase IV (Merck Life Science) for 140 min at 4°C. The resulting cell suspensions were filtered through cell strainers (Greiner) and centrifuged. Cells were washed, resuspended in DMEM supplemented with thioguanine (10 µg/mL, Merck Life Science), and plated in 100 mm^3 culture dishes at dilutions of 1:2, 1:10 and 1:100. After 2 weeks of incubation, colonies were fixed with methanol and visualized by crystal violet staining.

India ink assay

Pulmonary metastatic burden was assessed following intratracheal administration of India ink (15% India ink, 85% water, 3 drops NH_4OH/100 mL). Lungs were subsequently immersed in Fekete's solution (300 mL 70% ethanol, 30 mL 37% formaldehyde, 5 mL glacial acetic acid). Metastatic nodules were identified as white foci contrasted against the blue-stained lung tissue and manually counted.

Stable 4T1-GFP generation

Green fluorescent protein (GFP) was inserted into the pLV-IRES-GFP bicistronic expression vector. Lentiviral particles were generated as previously described [27] using HEK293T cells transfected with pMDLg/pRRE, pMD2.VSVG, pRSV-Rev and pLV-IRES-GFP plasmids. Forty-eight hours after transfection, supernatants were collected, filtered and ultracentrifuged for 1 hour 30 min at 100,000×g. Viral pellets were resuspended and used to transduce 4T1 cells following viral titration. Stable GFP-expressing 4T1 cells were obtained, and GFP expression was confirmed by immunocytochemical staining and western blot analysis.

Cell isolation for RNA sequencing

After euthanasia, tumor tissues from IgG1-treated and C269-treated mice were processed to isolate 4T1 clone 5-GFP cells as well as CD4+ and CD8+ tumor-infiltrating T lymphocytes. Tumors were mechanically fragmented and enzymatically digested with collagenase (0.5 mg/mL) for 1 hour under continuous agitation. Dead cells were eliminated using the Dead Cell Removal Kit (Miltenyi). CD4+ and CD8+ tumor-infiltrating lymphocytes (TILs) were isolated by positive magnetic selection using mouse CD4 and CD8 MicroBeads (Miltenyi). GFP-positive 4T1 cells were purified from single-cell suspensions using an S3e Cell Sorter (Bio-Rad). Isolated cell pellets were washed, and total RNA was extracted using the SPLIT RNA Extraction Kit (Lexogen, Vienna, Austria).

RNA sequencing and data analysis

RNA sequencing libraries were prepared from total RNA isolated from 4T1-GFP cells and CD4+ and CD8+ TILs (five samples per experimental condition) derived from IgG1-treated and C269-treated tumors. RNA quality was assessed using the Agilent 2100 Bioanalyzer.

Library preparation was carried out using the QuantSeq 3′ mRNA-Seq Library Prep Kit (Lexogen, Vienna, Austria), followed by sequencing on an Illumina NextSeq 500 platform. Sequencing reads were normalized according to effective library size, and differential gene expression analysis was performed using DESeq version 2.21. Genes were considered differentially expressed when meeting a false discovery rate (FDR) threshold <0.05 and an absolute fold change >1.

Functional annotation and pathway enrichment of differentially expressed genes (DEGs) were conducted using DAVID version 6.8 and the Panther Classification System version 12.0. The RNA sequencing dataset was deposited in the Gene Expression Omnibus under accession number GSE223539.

Subsequently, mRNA accession numbers corresponding to DEGs were analyzed for transcription factor binding motif enrichment within regions spanning −950 bp to +50 bp relative to transcription start sites using Pscan [28] in combination with the JASPAR database.

Wound healing assay

Once 4T1-clone 5 cells reached complete confluence, a cross-shaped wound was introduced using a pipette tip. Cultures were rinsed twice with PBS to eliminate detached cells and debris. Cells were subsequently exposed for 24 hours to eNAMPT (500 ng/mL), control IgG1 (10 µg/mL), C269 (10 µg/mL), or ALT-200 (10 µg/mL). Images of the same wound region were captured at predefined time points. Wound closure was quantified by calculating the remaining open area using ImageJ software (National Institutes of Health, Maryland, USA).

Cell viability assay

Cell survival following exposure of 4T1 cells to eNAMPT, control IgG1, C269, or ALT-200 (10 µg/mL) was assessed using the colorimetric 3-(4,5-dimethylthiazol-2-yl)−2,5-diphenyltetrazolium bromide (MTT) assay. Cells were seeded in 24-well plates and

treated for the indicated durations. Vehicle was added where appropriate, ensuring a final concentration not exceeding 0.1%. MTT reagent (250 µg/mL in Locke buffer) was added and incubation was carried out for 1 hour at 37°C. Formazan precipitates were solubilized in isopropanol containing 0.1 m HCl, and absorbance was measured at 570 nm using a Victor3 V plate reader (PerkinElmer Life Sciences).

T-cell isolation

Naive CD4+ and CD8+ T lymphocytes were isolated from the spleens of healthy mice using the mouse naive CD4+ and CD8+ T Cell Isolation Kit (Miltenyi) and employed for in vitro assays. Regulatory T cells (Tregs) used in suppression experiments were obtained by sorting CD4+CD25+ cells from tumor-derived single-cell suspensions.

3D culture and co-culture

Three-dimensional 4T1 spheroids were generated by seeding 10^4 cells per well in V-bottom 96-well plates containing complete MEM. After 5 days, spheroids were co-cultured with 3×10^5 CD4+, CD8+, or combined CD4+/CD8+ T cells per well, in the presence of either control IgG1 or C269. Six replicate wells were prepared for each condition. For quantitative PCR (qPCR) and flow cytometric analyses, OUT and IN fractions were separated by pooling six wells into 1.5 mL tubes. Spheroids were gently resuspended and allowed to settle by gravity. The supernatant containing non-infiltrating immune cells was collected as the OUT fraction. This washing procedure was repeated twice with PBS. Spheroids were then enzymatically dissociated with trypsin to generate single-cell suspensions corresponding to the IN fraction, which were subsequently analyzed by qPCR and flow cytometry.

Spheroid volume calculation

Prior to trypsin digestion, pooled spheroids were transferred to 96-well plates and imaged using a Leica THUNDER Imager 3D Live Cell microscope (Wetzlar, Germany; objective 5×). Spheroid dimensions were determined with Icy software by measuring length (L) and width (W). Volumes were calculated using the formula $V = (L \times W \times W) / 2$, as previously described by Courau *et al*. [29].

T-cell infiltration calculation

To assess lymphocyte infiltration, 4T1-GFP spheroids were co-cultured with T cells labeled using CellTracker Red CMTPX Dye (Thermo Fisher Scientific), following established protocols. Imaging was performed using a Leica THUNDER Imager 3D Live Cell microscope (Wetzlar, Germany; objective 5×). Regions of interest (ROIs) were defined and quantified using Icy software.

T-cell proliferation and suppression assays

Lymph nodes and spleens were collected from IgG1-treated and C269-treated mice and processed to generate single-cell suspensions. CD3+ T cells were purified after depletion of B220+, CD11b+, CD49b+ and Ter-119+ populations, followed by sorting of CD4+CD25+ cells from tumor lysates. Purified CD3+ T cells (50×10^3 cells/well) were cultured in 96-well plates and stimulated with anti-CD3 antibody (1 µg/mL) or left unstimulated in enriched Roswell Park Memorial Institute (RPMI) 1640 medium. Cultures contained 500×10^3 splenocytes from naive mice as a source of antigen-presenting cells (APCs). After 72 hours at 37°C in 5% CO_2, cells were pulsed for 18 hours with 0.5 µCi/well [H^3]-thymidine. Proliferation was quantified from triplicate wells using a β-counter (Perkin Elmer, Waltham, Massachusetts, USA). Results are reported as mean cpm ± sem.

Flow cytometry

Primary tumors were mechanically fragmented and enzymatically digested using collagenase (0.5 mg/mL) for 1 hour under agitation. Cells (10^6) were resuspended in Hank's Balanced Salt Solution supplemented with 0.5% bovine serum albumin (BSA) and stained with specific antibodies for 30 min at 4°C. Cell viability was assessed using the LIVE/DEAD Fixable Violet Dead Cell Stain Kit. Intracellular staining was performed using the Foxp3/Transcription Factor Staining Buffer Set according to the manufacturer's protocol. Data acquisition was carried out on BD FACSCanto II or BD FACSymphony A5 cytometers and analyzed with BD FACSDiva and FlowJo (9.3.2) software.

Viability was determined with BD Horizon Fixable Viability Stain. Intracellular labeling employed the BD Cytofix/Cytoperm Fixation/Permeabilization Solution Kit following the manufacturer's instructions. Samples were acquired on a BD Symphony instrument and analyzed using BD FACSDiva V.8.0.2 and FlowJo (10.6.1) software.

Gene expression analysis

Total RNA was isolated by cell lysis in Trizol reagent (Life Technologies) followed by phase separation using chloroform. Reverse transcription was performed starting from 1 µg RNA using the SENSIFAST kit according to the manufacturer's instructions (Aurogene). Quantitative PCR was carried out using 20 ng cDNA with SYBR Green chemistry (Bio-Rad) on a CFX96 Real-Time PCR System (Bio-Rad). Relative transcript abundance was calculated after normalization to actin, used as the reference gene.

Immunohistochemical and immunofluorescence analysis

At the experimental endpoint, animals were euthanized and tumor tissues were excised. Paraffin-embedded tumors were sectioned at 4 µm thickness, deparaffinized and rehydrated. Antigen retrieval was performed using Novocastra Epitope Retrieval Solutions in a thermostatically controlled bath at 95°C for 15 min. Sections were cooled to room temperature, rinsed in PBS, endogenous peroxidase activity was quenched with H_2O_2, and Fc receptors were blocked using a dedicated protein solution. Slides were incubated overnight at 4°C with primary antibodies. Detection was achieved using IgG (H&L)–specific secondary antibodies (Life Technologies) and 3–3′ diaminobenzidine (DAB) substrate. Nuclear counterstaining was performed with Harris haematoxylin (Novocastra). Microscopic evaluation was carried out using a Leica DM4 B optical microscope equipped with a Leica DFC450 digital camera.

Immunofluorescence staining was conducted on frozen samples embedded in optimal cutting temperature (OCT) compound. For intracellular granzyme b detection, 4 µm sections were fixed in 4% paraformaldehyde and permeabilized with 0.1% Triton X-100, whereas membrane antigen staining was performed after fixation with cold acetone. Blocking was carried out in PBS 1× containing 5% BSA, followed by incubation with primary antibodies for 1 hour. Nuclear staining was performed using 4′,6-diamidino-2-phenylindole (DAPI). Confocal imaging was acquired using a Leica TCS-SP8-X laser scanning confocal microscope.

eNAMPT-neutralizing murine (C269) and humanized mAbs (ALT-200)

Production and purification of the murine anti-eNAMPT monoclonal antibody C269 were previously reported [15]. The humanized eNAMPT-blocking antibody ALT-200 was supplied by Aqualung Therapeutics Corporation (Tucson, Arizona, USA) [13, 30, 31].

Western blot analysis

Protein extracts from 4T1 cells and primary tumor tissues were prepared using lysis buffer containing 20 mM HEPES, 100 mM NaCl, 5 mM EDTA, 1% Nonidet-P40 and Protease & Phosphatase Inhibitor Cocktail (Sigma). Protein concentration was determined by Bradford assay (Sigma). Equal protein amounts were resolved by SDS–PAGE and transferred using the TurboBlot system (Bio-Rad, Hemel Hempstead, UK). Immunodetection was performed using specific primary antibodies followed by peroxidase-conjugated secondary antibodies (Bio-Rad), and signal development was achieved via enhanced chemiluminescence (ECL, Thermo Fisher Scientific). Band quantification was performed using Image Lab software (Bio-Rad, Hemel Hempstead, UK). Mouse anti-β-actin antibody A1978 was obtained from Sigma; rabbit anti-CTLA4 (clone VU-ID9) and anti-ICOS antibodies were purchased from Biorbyt; rabbit anti-ICOSL antibody was from Abbexa; rabbit anti-PD-1/CD279 polyclonal antibody 66-220–1-Ig and anti-PD-L1/CD274 monoclonal antibody 66-248–1-Ig were from Proteintech.

Recombinant NAMPT production

Endotoxin-free recombinant NAMPT protein was produced and purified in-house following previously published protocols [15, 32].

ELISA

Circulating eNAMPT concentrations in serum samples were quantified using a commercially available murine NAMPT sandwich ELISA kit (AdipoGen, Seoul, Korea).

Statistics

Results are expressed as mean ± SEM. Distribution normality was assessed using the Shapiro–Wilk test. Depending on data distribution, parametric tests (unpaired t-test or one-way ANOVA with Tukey's post-hoc test) or non-parametric tests (Mann–Whitney U test or Kruskal–Wallis H test followed by Dunn's post-hoc analysis) were applied. All statistical analyses were two-tailed, and p values <0.05 were considered statistically significant. Data processing and statistical calculations were performed using GraphPad Prism software (GraphPad Software, USA).

Results and Discussion

Neutralisation of eNAMPT limits TNBC progression in vivo

To define the role of extracellular NAMPT (eNAMPT) during TNBC development, we initially evaluated the impact of the murine eNAMPT-blocking monoclonal antibody C269 (IgG1κ [15, 16]) using the 4T1 syngeneic breast cancer model. Animals received intraperitoneal C269 administration twice weekly (2.5 mg/kg) beginning on day 1 following tumor implantation **(Figure 1a).** Consistent with observations reported in breast cancer patients [12], serum eNAMPT concentrations in tumor-bearing mice increased by more than 10-fold by day 28 relative to healthy controls **(Figure 1b).** In contrast, animals treated with C269 displayed substantially reduced circulating eNAMPT levels.

C269 exposure resulted in a marked suppression of tumor development, with both tumor volume (median 0.45 cm^3 vs 0.17 cm^3) and tumor mass (median 640.6 mg vs 435.7 mg) significantly decreased at endpoint **(Figures 1c–1e).** In parallel, the pronounced splenomegaly observed in tumor-bearing mice was significantly attenuated following C269 treatment **(Figure 1f)**. Moreover, quantification of metastatic spread using a clonogenic assay revealed a significant reduction in lung metastases in the C269-treated group **(Figure 1g)**.

Notably, therapeutic benefit was also observed when C269 administration was initiated after tumor establishment. When treatment was started once tumors became palpable (approximately 14–16 days post-implantation, following randomization); **(Figure 1h)**, C269 significantly decreased tumor volume (median 0.36 cm^3 vs 0.10 cm^3) and tumor weight (median 486.5 mg vs 368 mg) **(Figures 1i and 1j).** This delayed-treatment regimen also reduced spleen enlargement **(Figure 1k)**, circulating eNAMPT concentrations **(Figure 1l),** and pulmonary metastatic burden **(Figure 1m).** Although raw measurements suggested a numerically greater response when therapy was initiated at the palpable stage compared with early intervention, statistical analysis revealed no significant difference between the two schedules, indicating comparable efficacy of C269 under both regimens. Importantly, administration of a non-specific IgG1 control antibody did not affect tumor growth relative to vehicle-treated animals.

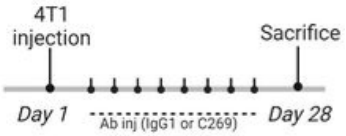

a)

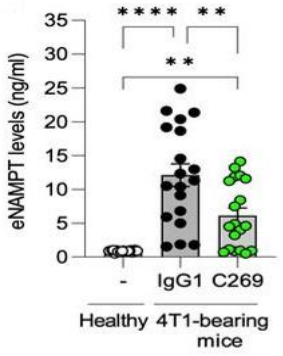

b)

c)

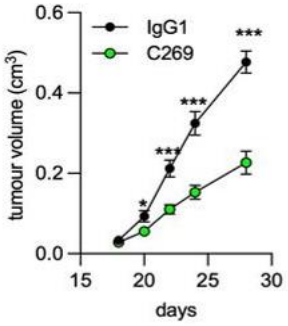

d)

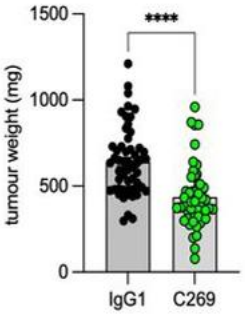

e)

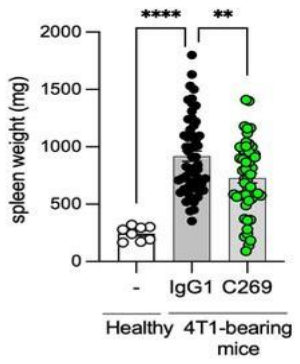

f)

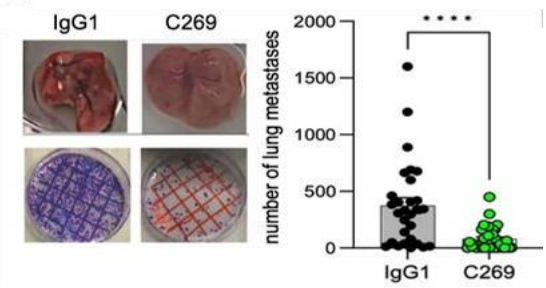

g)

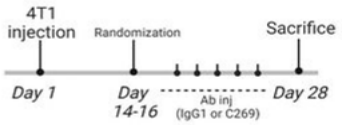

h)

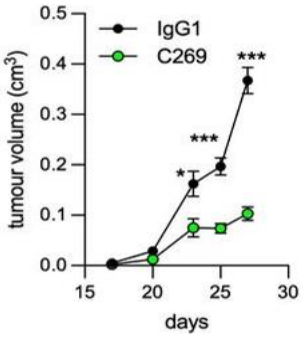

i)

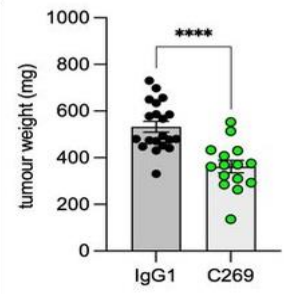

j)

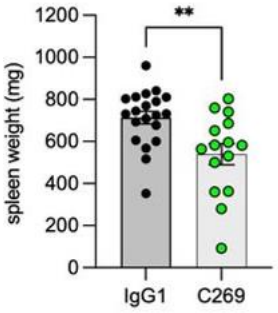

k)

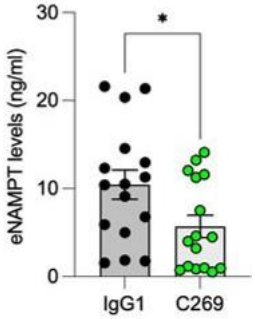

l)

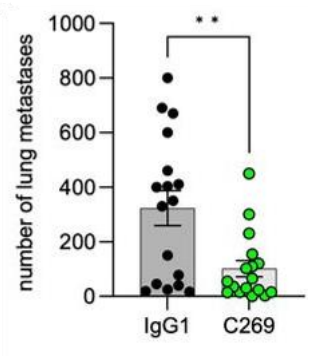

m)

n)

Figure 1. eNAMPT blockade suppresses 4T1 tumor growth and metastatic dissemination.
(a) Experimental design corresponding to panels B–G. 4T1 cells were orthotopically implanted into the mammary fat pad of female BALB/c mice. Animals received intraperitoneal injections of control IgG1 (2.5 mg/kg, twice weekly) or C269 (2.5 mg/kg, twice weekly).

(b) Serum eNAMPT concentrations in healthy mice and in IgG1- or C269-treated 4T1-bearing mice.
(c) Representative images of excised 4T1 tumors.
(d) Tumor volume progression over time.
(e) Tumor weight at sacrifice.
(f) Spleen weight at sacrifice compared with age- and weight-matched controls.
(g) Lung metastatic burden assessed by the 6-thioguanine clonogenic assay. Mean ± SEM from eight independent experiments.
(h) Treatment scheme for data shown in panels I–M. Control IgG1 (2.5 mg/kg, i.p., twice weekly) or C269 (2.5 mg/kg, i.p., twice weekly) was administered after tumors became palpable (≈day 15).
(i) Tumor volume kinetics.
(j) Tumor weight at sacrifice.
(k) Spleen weight at sacrifice.
(l) Serum eNAMPT levels at endpoint.
(m) Lung metastases quantified by the 6-thioguanine clonogenic assay.
(n) Number of lung metastatic nodules following tail-vein injection of 4T1 cells in mice treated or not treated with C269. Mean ± SEM from three independent experiments (panels H–N).
*p<0.05; **p<0.01; ***p<0.001; ****p<0.0001.
eNAMPT, extracellular nicotinamide phosphoribosyltransferase; i.p., intraperitoneal.

Because metastatic burden can be influenced by primary tumor size, we next assessed whether C269 directly affected metastatic colonization independently of primary tumor growth. To this end, identical numbers of 4T1 cells were injected intravenously via the tail vein into treated and untreated mice and allowed to disseminate for 28 days. Under these conditions, C269-treated mice developed significantly fewer lung metastases than control animals **(Figure 1n).**

To further validate the susceptibility of TNBC to eNAMPT inhibition, we extended our analysis in two additional ways: (1) evaluation of C269 efficacy in a second TNBC model (EO771); and (2) testing of an independent humanized eNAMPT-neutralizing antibody. As expected, EO771-bearing mice exhibited elevated circulating eNAMPT levels, and C269 treatment produced antitumor effects comparable to those observed in the 4T1 model, with the exception of splenomegaly, which was not evident in EO771-bearing mice. Further confirmation of target relevance was obtained using the humanized anti-eNAMPT antibody ALT-200 [13, 30, 31], which also significantly inhibited 4T1 tumor growth and dissemination.

eNAMPT does not directly drive tumor cell proliferation in vitro

To examine whether eNAMPT acts autonomously to support proliferation or prevent death in tumor cells, we treated 4T1 cultures with recombinant murine NAMPT (rNAMPT). Across all tested concentrations (10 ng/mL to 1 µg/mL) and time points (24–96 hours), rNAMPT exposure did not affect cell growth in conventional monolayer cultures. Similarly, 4T1 spheroids showed no measurable changes in proliferation under the same conditions. Since 4T1 cells naturally release substantial amounts of eNAMPT (approximately 2.8 ng accumulated over 24 hours from 1×10^6 cells, quantified by ELISA and corroborated by western blot), it is possible that this endogenous secretion obscures any additional effect. Nonetheless, administration of the eNAMPT-neutralizing antibodies C269 or ALT-200 did not influence proliferation or cell viability in either monolayer or spheroid systems at any evaluated time point.

Transcriptional changes induced by eNAMPT blockade in 4T1 cells

To investigate the impact of eNAMPT inhibition on gene expression, RNA-sequencing was performed on 4T1 cells isolated from tumors following 28 days of treatment with either control IgG1 or C269, administered from day 1. To obtain a pure tumor cell population, 4T1 cells were genetically modified to express GFP constitutively (GFP-4T1), **(Figure 2a),** allowing separation by flow cytometry. These GFP-4T1 cells responded to C269 treatment similarly to unmodified 4T1 cells in terms of tumor volume, weight, splenomegaly, and lung metastasis.

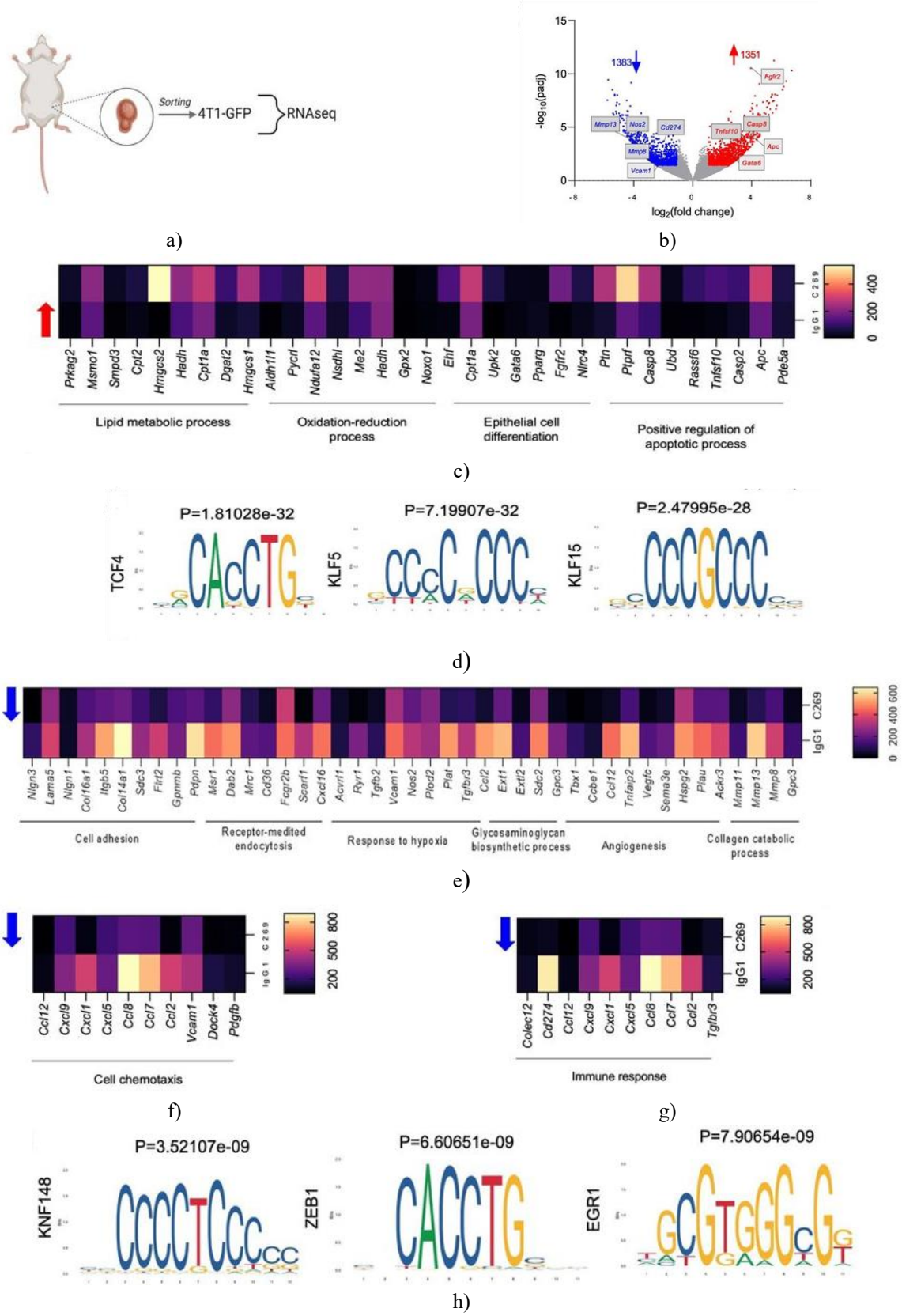

a) b) c) d) e) f) g) h)

Figure 2. Transcriptomic profiling of 4T1 cells isolated from tumors

(a) Illustration of GFP-4T1 cells retrieved from tumor masses and processed for RNA sequencing analysis. (b) Volcano plot depicting genes differentially expressed in 4T1clone5-GFP cells (n=5 per condition; FDR ≤ 0.05). (c) Heat map and bar graph showing genes with increased expression following C269 treatment, with associated GO pathway analysis. (d) Enriched transcription factor motifs in promoters of genes upregulated in response to C269. (e–g) Heat maps and histograms of genes whose expression decreased after C269 exposure, alongside GO pathway enrichment. (h) Transcription factor motifs enriched in promoters of downregulated genes. FDR, false discovery rate; GO, gene ontology; RNAseq, RNA sequencing.

Upon comparison with IgG1-treated tumors, administration of C269 led to 1,351 genes being upregulated and 1,383 downregulated **(Figure 2b),** applying a $\log_2$ fold-change ≥1 and FDR < 0.05. qPCR validation on GFP-4T1clone 5 cells extracted from tumors confirmed the RNAseq results with a correlation of 0.94. **Figure 2c** visualizes the four most enriched pathways after C269 treatment according to GO analysis, representing genes affected by eNAMPT depletion.

To assess whether the observed upregulation occurred independently of the tumor microenvironment, cultured 4T1 cells were exposed to rNAMPT and expression of key genes was measured. Certain genes (e.g., Gata6, Ptn) showed similar responses in vitro, while others, particularly apoptosis-related genes, did not. Transcription factor motif analysis via Pscan and JASPAR suggested TCF4, KLF5, and KLF15 as likely regulators for the upregulated genes **(Figure 2d).**

Figures 2e–g display the eight top pathways affected, with KNF148, ZEB1, and EGR1 as predicted key transcription factors **(Figure 2h).** Notably, genes related to chemotaxis and adhesion were strongly reduced, potentially underlying the lower metastatic load in C269-treated tumors and cells **(Figures 1g and 1n).** Most of these effects appear cell-autonomous: 11 of 13 genes tested in monolayer 4T1 cultures responded similarly to rNAMPT treatment, whereas two genes (Lama5 and Mmp11) did not, indicating both intrinsic and context-dependent regulation by eNAMPT.

Functional validation was performed by analyzing wound closure in vitro. rNAMPT increased 4T1 migration in a dose-dependent manner, whereas both C269 and ALT-200 suppressed basal migration, supporting that eNAMPT functions as an autocrine signal promoting motility in mammary carcinoma cells.

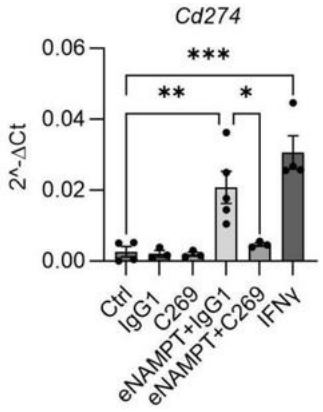

a)

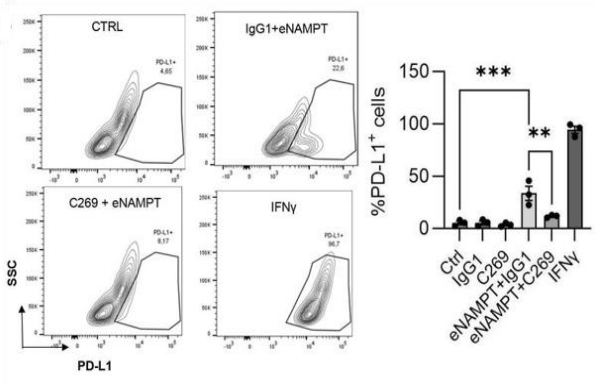

b)

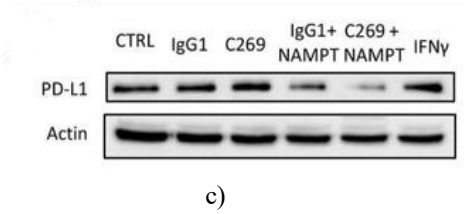

c)

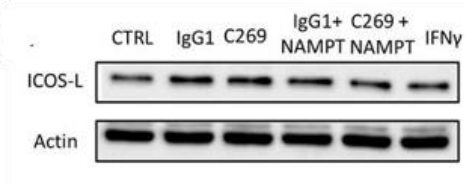

d)

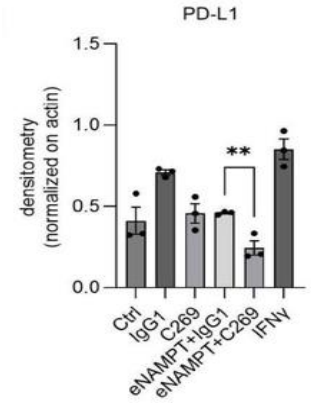

e)

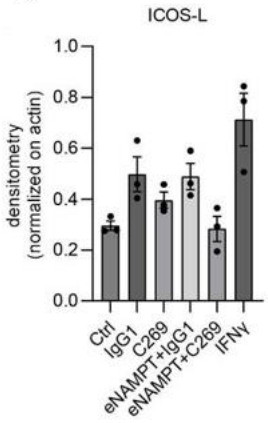

f)

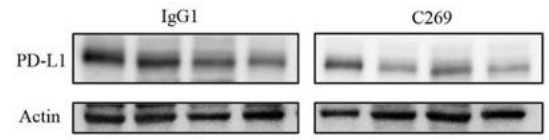

g)

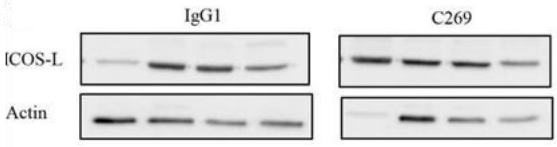

h)

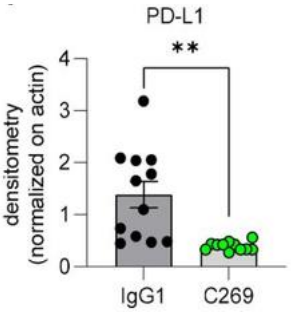

i)

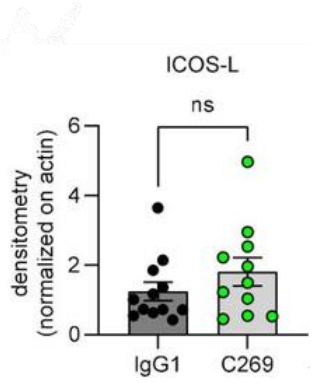

j)

Figure 3. Effects of eNAMPT neutralization on the PD-L1 signaling in tumor cells**.** (a–b) Expression of Cd274 and PD-L1 analyzed by qPCR and FACS in 4T1 cells exposed to eNAMPT (500 ng/mL) alone or together with C269 (10 µg/mL). IFNγ (100 ng/mL) was included as a positive control. Data are shown as mean±SEM from three separate experiments. (c–d) Representative western blot and (e–f) densitometric analysis of PD-L1 and ICOS-L in total cell lysates of 4T1 cells treated with rNAMPT for 24 hours. Mean±SEM from three independent experiments. (G–H) Representative western blot and (i–j) densitometry of PD-L1 and ICOS-L from homogenized tumors of 4T1-bearing mice. Mean±SEM of 12 samples obtained from two independent experiments. Abbreviations: eNAMPT, extracellular nicotinamide phosphoribosyltransferase; FACS, fluorescence-activated cell sorting; ICOS, inducible T-cell costimulator; IFN, interferon; PD-L1, programmed death-ligand 1; qPCR, quantitative PCR; rNAMPT, recombinant murine NAMPT; SSC, side scatter [1–2].

Neutralization of eNAMPT influences T-cell programming

Analysis of RNAseq data from GFP-4T1 cells extracted from tumors showed that genes involved in tumor-immune interactions, such as CD274 (PD-L1), were strongly downregulated when treated with C269 **(Figure 2g)** [3]. This effect was intrinsic to the tumor cells: applying rNAMPT in vitro to 4T1 cultures increased PD-L1 mRNA **(Figure 3a)** and protein **(Figures 3b–3c),** which was reversed by co-treatment with C269 **(Figures 3a, 3b, and 3e),** without altering ICOS-L expression **(Figures 3d and 3f)** [4]. The inhibitory impact of C269 on PD-L1 protein was also confirmed in vivo in tumor homogenates from 4T1 **(Figures 3g–3j)** and EO771 allografts [5]. Notably, in both tumor models, reductions in PD-L1 were accompanied by decreased PD-1 levels

(Figures 4a and 4c), while ICOS remained unaffected **(Figure 4b and 4d)** [6].

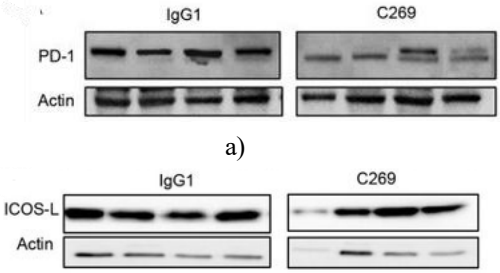

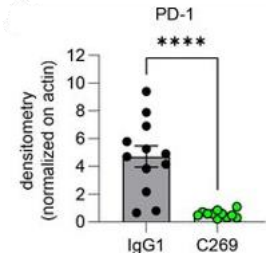

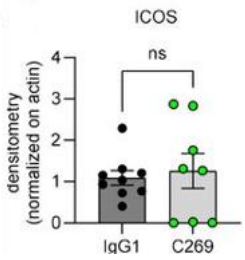

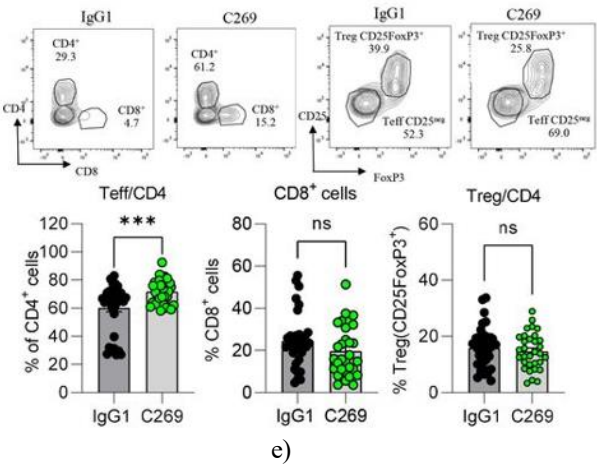

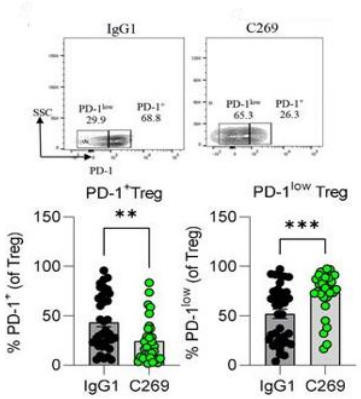

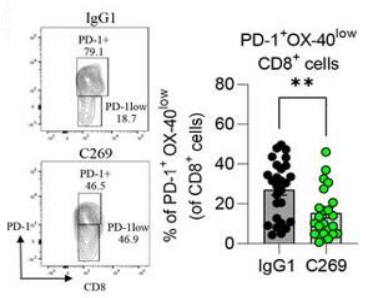

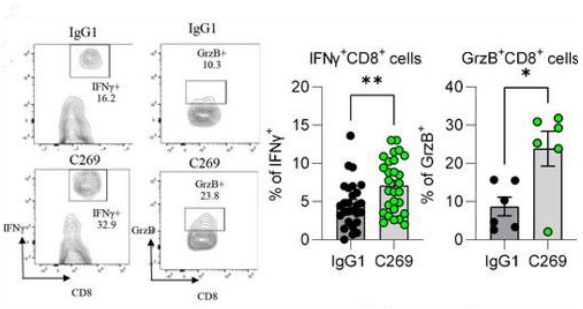

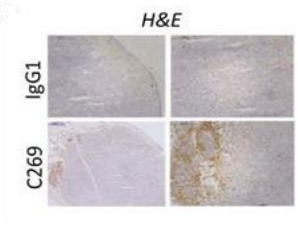

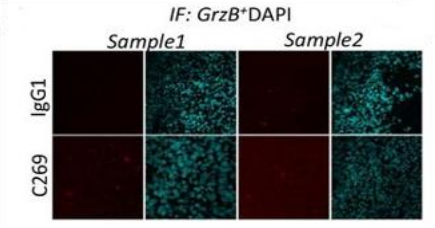

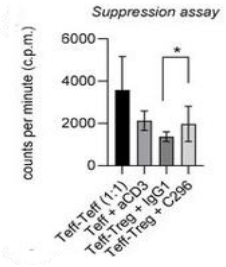

k)

l)

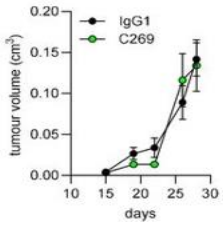

m)

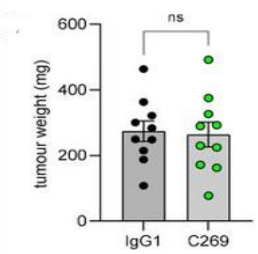

n)

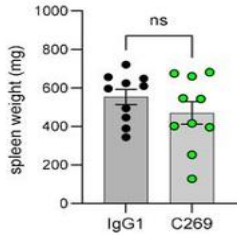

o)

Figure 4. Impact of eNAMPT neutralization on the PD-1/PD-L1 pathway in the tumor milieu**.** (a–b) Example western blots and (c–d) corresponding densitometric analyses of PD-1 and ICOS in homogenates from 4T1 tumors. Data represent mean±SEM from 12 samples across two separate experiments. (e–h) Immune cell quantification: (e) T effector cells, T regulatory cells (CD4+ gated) and CD8+ cells; (F) PD-1+ Tregs (CD4+CD25+FoxP3+ gated); (g) PD-1+CD8+ T cells (CD8+ gated); (H) CD8+ T cells expressing IFN and GrzB (CD8+ gated). Data shown as mean±SEM from five independent experiments. (i) IHC staining of CD8+ T cells in tumor sections. (j) Immunofluorescence visualization of GrzB+ in CD8+ T cells. (k) Treg suppression assessed by [^{3}H]-thymidine incorporation from spleen and draining lymph nodes. Mean±SEM of three experiments. Statistical significance: *p<0.05; **p<0.01; ***p<0.001; ****p<0.0001. (L–O) 4T1 cells implanted intramammarily in female nude BALB/c mice. Mice received control IgG1 (2.5 mg/kg i.p., twice weekly) or C269 (2.5 mg/kg i.p., twice weekly). (l) Representative tumor images; (M) tumor growth over time; (n) tumor weight at endpoint; (o) spleen weight at endpoint and in age- and weight-matched controls. Data are mean±SEM from a single experiment. Abbreviations: DAPI, 4’,6-diamidino-2-phenylindole; eNAMPT, extracellular nicotinamide phosphoribosyltransferase; GrzB, granzyme B; ICOS-L, inducible T-cell costimulator ligand; IFN, interferon; IHC, immunohistochemistry; i.p., intraperitoneal; PD-1, programmed cell death protein 1; PD-L1, programmed death-ligand 1; Teff, T effector cells; Treg, regulatory T cell [1–2].

Because PD-1 is predominantly expressed by T and pro-B lymphocytes, we evaluated both lymphoid and myeloid populations from tumors 28 days post-treatment with either IgG1 or C269. C269 did not significantly alter myeloid or B cell compartments. However, marked differences were observed in lymphoid composition: CD4+CD25neg effector cells were more abundant in C269-treated tumors, while Treg (CD4+CD25+FoxP3+) and CD8+ cell frequencies remained unchanged **(Figure 4e).**

Further phenotyping revealed that C269 reduced PD-1+ Tregs and PD-1+CD8+ T cells **(Figure 4f),** while PD-1low Tregs and CD8+ IFN+GrzB+ cytotoxic cells increased **(Figures 4g and 4h).** Markers such as CD73 or OX40 did not differ in Teffs, Tregs, or CD8+ populations . These changes were also confirmed in EO771 tumors, indicating consistent T-cell remodeling across models. Collectively, these results suggest that C269 enhances CD8+ cytotoxic activity. Supporting this, IHC demonstrated deeper infiltration of CD8+ cells into tumor stroma under C269 **(Figure 4i),** and immunofluorescence confirmed these cells expressed GrzB **(Figure 4j).** While PD-1low Tregs increased, which is typically associated with immunosuppression [33], functional assays ([^{3}H]-thymidine incorporation) showed that Tregs from C269-treated mice had reduced suppressive capacity **(Figure 4k).**

To assess whether T cells are essential for eNAMPT neutralization effects, 4T1 tumors were implanted in T-cell-deficient nude mice. Tumor growth, weight, and spleen size were unaffected by **C269 (Figures 4l–4o),** confirming that T cells are required to mediate the response.

eNAMPT regulates T-cell infiltration and activity

To explore underlying mechanisms, CD4+ and CD8+ T cells were isolated from 4T1 tumors for RNAseq analysis **(Figure 5a)**. Using log2 fold-change ≥1 and FDR<0.05, 65 and 112 genes were upregulated in CD4+ and CD8+ cells, respectively, while 158 and 92 genes were downregulated. These findings were validated by qPCR, showing a correlation of 0.84[4–6].

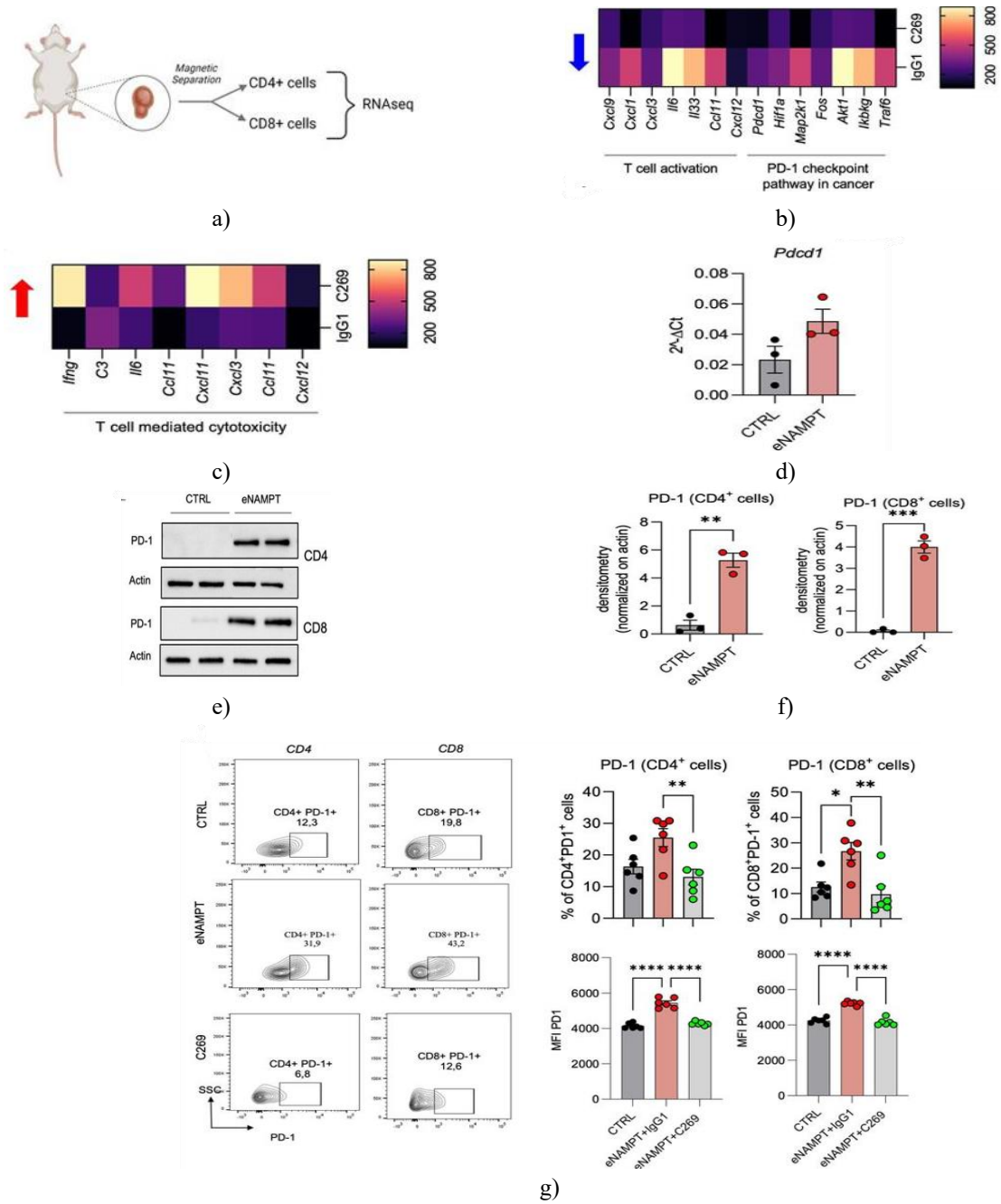

Figure 5. C269 reprograms tumor-infiltrating T-cell profiles. (a) Schematic representation of CD4+ and CD8+ T cells harvested from 4T1 tumors and subjected to RNA sequencing. (b) Heatmap and histogram illustrating genes

suppressed in CD4+ cells following C269 administration and the corresponding GO enrichment. (c) Heatmap and histogram showing genes upregulated in CD8+ cells upon C269 treatment, with related GO analysis. (d) Quantification of Pdcd1 (PD-1) transcripts by qPCR in T cells treated with eNAMPT (500 ng/mL). Data are mean±SEM from three independent experiments. (e–f) Representative western blot images and densitometric analysis of PD-1 protein in CD4+ and CD8+ T cells after 24-hour exposure to rNAMPT. (g) PD-1 protein levels in T cells initially treated with eNAMPT for 24 hours, followed by 24-hour neutralization with C269. Mean±SEM of three independent experiments. Statistical significance: **p<0.01; ***p<0.001. Abbreviations: eNAMPT, extracellular nicotinamide phosphoribosyltransferase; GO, gene ontology; PD-1, programmed cell death protein 1; qPCR, quantitative PCR; RNAseq, RNA sequencing; rNAMPT, recombinant murine NAMPT; SSC, side scatter [1–2].

Figure 5b highlight the two most significantly downregulated pathways in CD4+ T cells after C269 treatment, as revealed by GO analysis. These included genes linked to PD-1 signaling, while no additional pathways showed notable suppression. Conversely, **Figure 5c** indicate that in CD8+ cells, upregulated genes enriched a single pathway related to cytotoxic T-cell activity, consistent with the in vivo results and flow cytometry data. These observations collectively indicate that neutralizing eNAMPT in tumor-bearing mice selectively diminishes PD-1 signaling while enhancing cytotoxic functionality.

To investigate whether circulating eNAMPT directly modulates T cells, lymphocytes from healthy mice were treated with rNAMPT. In both CD4+ and CD8+ T cells, exposure to rNAMPT (500 ng/mL, 24 hours) elevated PD-1 mRNA and protein levels **(Figures 5d–5f).** Similarly, naive lymphocytes incubated with eNAMPT for 48 hours showed increased PD-1 expression. Importantly, when cells were incubated with eNAMPT for 24 hours and then co-treated with C269 for an additional 24 hours, the PD-1 increase was fully reversed in both T-cell subsets **(Figure 5g).** In line with these effects, rNAMPT also upregulated Cxcl1, Cxcl9, Il6, and Hif1a in CD4+ cells, and Ifng, Il6, and Cxcl11 in CD8+ cells.

To assess whether PD-1/PD-L1 blockade would add to C269 effects, 4T1-bearing mice were treated at days 4, 8, and 12 post-engraftment with anti-PD-1 (2 mg/kg) or anti-PD-L1 (2 mg/kg) antibodies, alone or in combination with C269 (every three days). Anti-PD-1 alone slightly but significantly reduced tumor growth and lung metastases, whereas anti-PD-L1 reduced metastases but not primary tumor volume. Co-treatment did not enhance outcomes. Unexpectedly, both anti-PD-1 and anti-PD-L1 partially counteracted C269's effect on primary tumor growth, although metastatic effects were unaffected, suggesting PD-1/PD-L1 signaling influences eNAMPT activity; both antibodies also significantly reduced systemic eNAMPT levels.

To determine whether eNAMPT impacts additional checkpoints, RNAseq datasets from CD4+ and CD8+ T cells were queried for Tim3, Lag3, Icos, Ctla4, and Ox40, with qPCR validation. No significant alterations were detected. Likewise, no changes were observed in Icosl, Cd274, or Cxcr4 expression in 4T1 tumor cells, confirming that eNAMPT specifically regulates the PD-1/PD-L1 axis, as corroborated by western blot and FACS. Finally, to evaluate functional consequences of transcriptional modulation, an in vitro 3D tumor-T-cell co-culture model was established. CD4+, CD8+, or combined T cells were pretreated with rNAMPT for 24 hours, washed, and incubated with naive 4T1 spheroids **(Figure 6a).** Immunofluorescence **(Figures 6b and 6c)** and flow cytometry **(Figure 6d)** revealed enhanced infiltration of rNAMPT-primed CD4+ cells into the spheroids. PD-1 levels increased in total CD4+ cells and Tregs (CD4+CD25+FoxP3+), whereas CD8+ cells and other functional markers were largely unaffected, indicating that increased infiltration occurs independently of PD-1 upregulation. The number of 4T1 cells within spheroids remained unchanged.

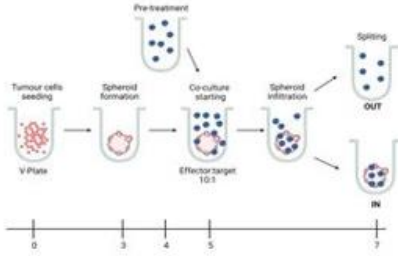

a)

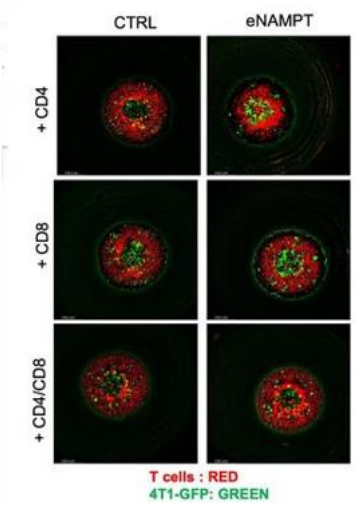
CTRL
eNAMPT
+ CD4
+ CD8
+ CD4/CD8
T cells : RED
4T1-GFP: GREEN

b)

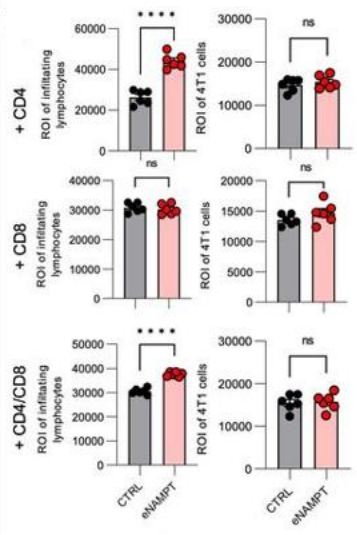
+ CD4
+ CD8
+ CD4/CD8
ROI of infiltating lymphocytes
ROI of 4T1 cells
ns
CTRL
eNAMPT

c)

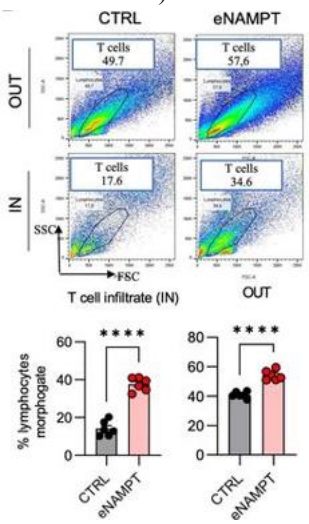
CTRL
eNAMPT
OUT
IN
T cells 49.7
T cells 57,6
T cells 17.6
T cells 34.6
SSC
FSC
T cell infiltrate (IN)
OUT
% lymphocytes morphogate

d)

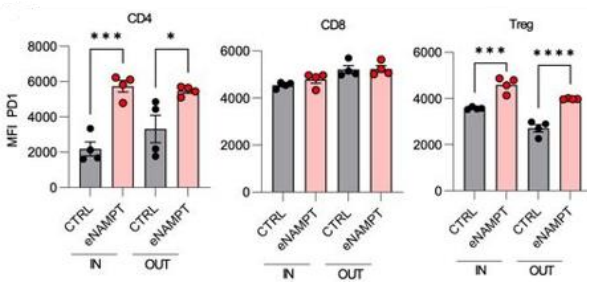
CD4
CD8
Treg
MFI PD1
IN
OUT
CTRL
eNAMPT

e)

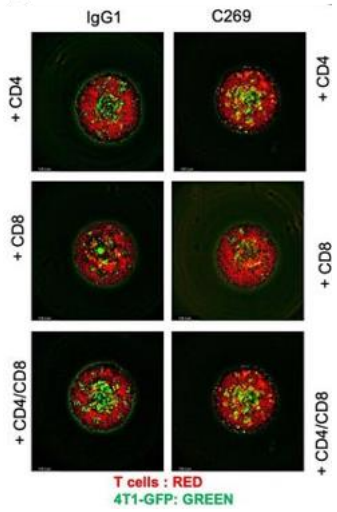
IgG1
C269
+ CD4
+ CD8
+ CD4/CD8
T cells : RED
4T1-GFP: GREEN

f)

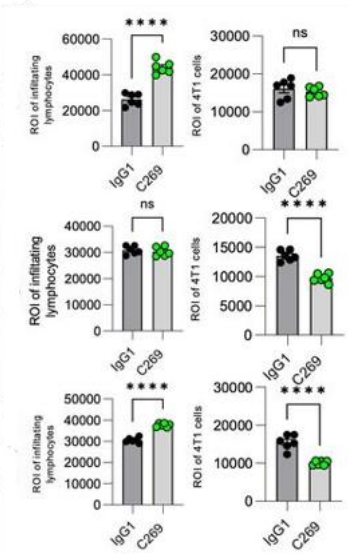
ROI of infiltating lymphocytes
ROI of 4T1 cells
ns
IgG1
C269

g)

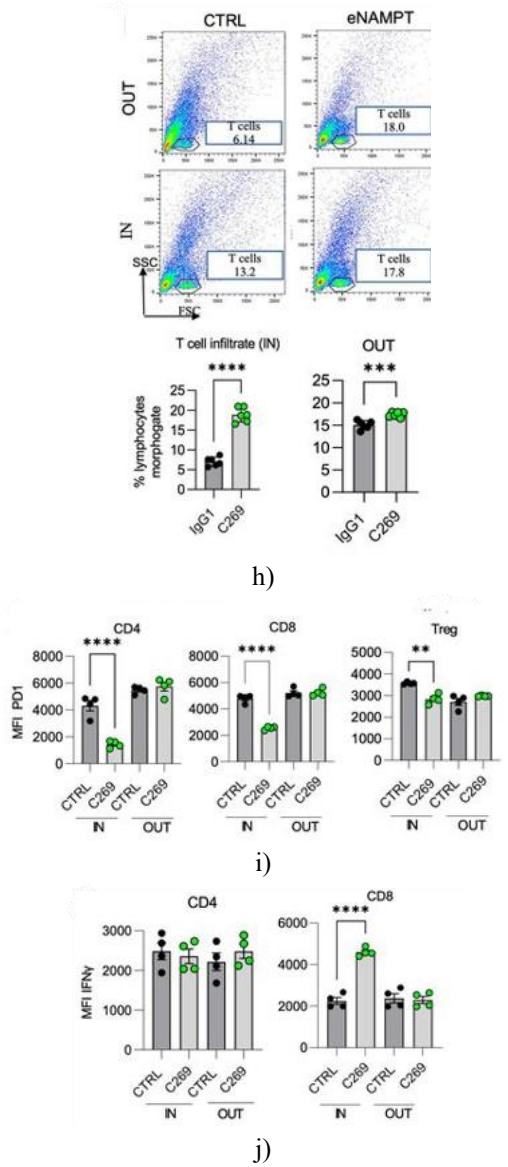

Figure 6. eNAMPT drives immunosuppressive features in T cells infiltrating 4T1 spheroids. (a) Overview of the experimental setup used in this figure. (b) Example immunofluorescence images and (c) quantification of regions of interest (ROI), displaying 4T1-GFP cells (green) and lymphocytes (red) within the spheroid. N=6; mean±SEM from two independent experiments. (d) Flow cytometry quantification of T-cell infiltration into spheroids. N=6; mean±SEM from two independent experiments. (e) Median fluorescence intensity (MFI) of PD-1 comparing cells located inside versus outside the spheroid. Mean±SEM from two experiments. (f) Representative immunofluorescence images and (g) ROI quantification showing the effect of C269 treatment on 4T1-GFP (green) and lymphocytes (red) within spheroids. Mean±SEM from three independent experiments. (h) Flow cytometry of T-cell penetration into spheroids after C269 treatment. N=6; mean±SEM of three experiments. (i) PD-1 MFI in IN and OUT spheroid compartments. Mean±SEM of three independent experiments. (j) IFNγ MFI in IN and OUT compartments. Mean±SEM of three experiments. Statistical significance: *p<0.05; **p<0.01; ***p<0.001; ****p<0.0001. Abbreviations: eNAMPT, extracellular nicotinamide phosphoribosyltransferase; IFN, interferon; MFI, median fluorescence intensity; PD-1, programmed cell death protein 1; ROI, region of interest [1, 2].

To explore how C269 influences lymphocyte behavior, T cells were co-cultured with 4T1 spheroids either in the presence or absence of the neutralizing antibody, using endogenous eNAMPT released from the tumor cells. Treatment with C269 markedly increased CD8+ cell infiltration into the spheroid **(Figures 6f and 6g)**. This infiltration coincided with a reduction in spheroid 4T1 cells, indicating that cytotoxic T-cell activity was restored. Importantly, infiltrating CD4+, CD8+, and Treg cells exhibited lower PD-1 levels compared to untreated controls, while expression of CD73 and OX40 remained unchanged. PD-1 in infiltrating lymphocytes was also lower than in non-infiltrating cells from the same culture. Functional validation confirmed that infiltrating lymphocytes produced IFNγ, demonstrating an activated cytotoxic state. These observations mirrored in vivo results, supporting the relevance of the spheroid model for C269-mediated effects. Interestingly, rNAMPT treatment paradoxically also increased T-cell infiltration **(Figures 6b–6e)**, similar to the effect of C269, but with a distinct phenotype. Both C269 and rNAMPT elevated CD4+ T-cell numbers, but rNAMPT preferentially expanded PD-1+ Tregs, potentially explaining the enhanced infiltration. Therefore, while the co-culture system effectively models C269 action, its predictions regarding rNAMPT effects are preliminary and hypothesis-generating.

Extracellular NAMPT (eNAMPT) represents the secreted form of the intracellular enzyme nicotinamide phosphoribosyltransferase, and is now recognized as a cytokine released by tumor cells, immune cells, and other stromal components, including adipocytes, fibroblasts, and endothelial cells. Numerous studies have reported elevated plasma levels of eNAMPT in patients with inflammatory disorders and malignancies [15, 34–36].

The specific cellular sources of eNAMPT in cancer remain unclear, though both tumor and immune cells display increased intracellular NAMPT expression [37, 38], which can be secreted through both brefeldin-dependent and independent mechanisms [6, 16, 39]. Recent work has identified TLR4 as one receptor engaged by extracellular eNAMPT, although it does not account for all of its signaling. For example, we recently demonstrated that eNAMPT can induce M1 macrophage polarization and drive migration even in TLR4-deficient mice [16]. In vitro, eNAMPT has been associated with enhanced proliferation [40–43] and epithelial-mesenchymal transition [44, 45], but its contribution in relevant in vivo cancer models has not been fully explored.

In this study, we first confirmed that serum eNAMPT is elevated in allograft models of triple-negative breast cancer. Using neutralizing antibodies (C269 and ALT-200), we observed that blocking eNAMPT reduced tumor growth and metastatic dissemination. Notably, eNAMPT did not directly support tumor cell proliferation or resistance to cell death, as neither recombinant cytokine nor neutralizing antibodies affected 2D or 3D 4T1 cultures. These findings partly contrast with previous reports of recombinant eNAMPT promoting proliferation in vitro, likely due to differences in cell lines [40–42]. Importantly, our data reveal that eNAMPT regulates PD-L1 expression on tumor cells and PD-1 on T lymphocytes, and that its neutralization restores antitumor immune activity. While we previously reported that intracellular NAMPT mobilizes immature myeloid-derived suppressor cells and enhances their suppressive activity, here we observed no effect of extracellular NAMPT blockade on myeloid populations. It is well established that intracellular NAMPT levels are increased in both cancer cells and tumor-associated immune cells [5, 46, 47], and intracellular NAMPT-dependent NAD synthesis has been linked to IFNγ-induced PD-L1 expression in tumor cells [38, 48]. This suggests a model in which intracellular NAMPT fuels cancer cell bioenergetics and supports myeloid immunosuppression, whereas secreted NAMPT modulates lymphoid immune evasion—a coordinated, tripartite mechanism in which intracellular NAMPT serves as the source of extracellular NAMPT, providing spatial and temporal control of tumor immune escape.

Notably, the regulation of PD-L1 on tumor cells and PD-1 on T lymphocytes appears to be cell-autonomous, as it can be reproduced in cultured tumor cells and in isolated T cells from healthy animals. Transcriptomic analyses of ex vivo CD4+ T cells demonstrated downregulation of genes associated with PD-1 signaling. Consistent with this, analysis of the tumor microenvironment revealed that C269 treatment enhanced cytotoxic T-cell activation (IFNγ+ and GrzB+) while reducing PD-1+ populations, thereby removing inhibitory constraints on T-cell cytotoxicity [48]. Moreover, C269 diminished the immunosuppressive activity of Tregs, as evidenced by functional assays and reductions in IL10+CD73+ Treg populations.

The central role of eNAMPT in controlling the PD-1/PD-L1 axis is further supported by the observation that co-treatment with C269 and anti-PD-1/PD-L1 antibodies did not yield additive effects on tumor growth or metastasis. Interestingly, these experiments also indicate a feedback loop, where PD-1/PD-L1 signaling promotes circulating eNAMPT levels, and blocking the checkpoint pathway abolishes C269's effect on primary tumors by preventing eNAMPT elevation.

Conclusion

In summary, targeting eNAMPT with neutralizing antibodies selectively reprograms T lymphocytes, restoring antitumor immunity, and represents a promising therapeutic strategy in triple-negative breast cancer.

Acknowledgments: We thank the Dr. Henrik Molina of the Proteomics Resource Center at Rockefeller University for the performance of all LC/MS-MS experiments. Molecular graphics and analyses performed with UCSF Chimera, developed by the Resource for Biocomputing, Visualization, and Informatics at the UCSF, with support from NIH P41-GM103311. We acknowledge the use of the MSK Flow Cytometry Core Facility, funded in part through the NIH/NCI Cancer Center Support Grant P30 CA008748. We thank Dr. Joshua Elias (Chan Zuckerberg Biohub, Stanford, CA, USA) for providing HLA typing of samples from PXD004746 and PXD005704.

Conflict of Interest: None

Financial Support: The research was supported by an AIRC grant to AAG (AIRC IG2018 21842) and SS (AIRC IG2018 22208; Project Code: 25323), a PRIN grant from the Italian Ministry of Health to AAG

(Ministero dell'Università e della Ricerca PRIN 2017 CBNCYT). An AIRC fellowship to GC (Project Code: 25323), a University of Pavia grant to CT (Università degli Studi di Pavia FRG-2019/2020), a Cariplo Foundation grant to CT (Fondazione Cariplo 2020-3598) and a PRIN grant from the Italian Ministry of Health to CT (Ministero dell'Università e della Ricerca PRIN 2020SEMP22).

Ethics Statement: None

References

1. Jiang Y, Chen M, Nie H, et al. PD-1 and PD-L1 in cancer Immunotherapy: clinical implications and future considerations. Hum Vaccin Immunother 2019;15:1111–22. 10.1080/21645515.2019.1571892
2. Kotanides H, Li Y, Malabunga M, et al. Bispecific targeting of PD-1 and PD-L1 enhances T-cell activation and antitumor immunity. Cancer Immunol Res 2020;8:1300–10. 10.1158/2326-6066.CIR-20-0304
3. Cui X, Jia H, Xin H, et al. A novel Bispecific antibody targeting PD-L1 and VEGF with combined anti-tumor activities. Front Immunol 2021;12:778978. 10.3389/fimmu.2021.778978
4. McGowan E, Lin Q, Ma G, et al. PD-1 disrupted CAR-T cells in the treatment of solid tumors: promises and challenges. Biomedicine & Pharmacotherapy 2020;121:109625. 10.1016/j.biopha.2019.109625
5. Travelli C, Consonni FM, Sangaletti S, et al. Nicotinamide Phosphoribosyltransferase acts as a metabolic gate for mobilization of myeloid-derived Suppressor cells. Cancer Research 2019;79:1938–51. 10.1158/0008-5472.CAN-18-1544
6. Grolla AA, Torretta S, Gnemmi I, et al. Nicotinamide Phosphoribosyltransferase (NAMPT/PBEF/Visfatin) is a Tumoural cytokine released from Melanoma. Pigment Cell Melanoma Res 2015;28:718–29. 10.1111/pcmr.12420
7. Galli U, Colombo G, Travelli C, et al. Recent advances in NAMPT inhibitors: A novel Immunotherapic strategy. Front Pharmacol 2020;11:656. 10.3389/fphar.2020.00656
8. Garten A, Schuster S, Penke M, et al. Physiological and pathophysiological roles of NAMPT and NAD metabolism. Nat Rev Endocrinol 2015;11:535–46. 10.1038/nrendo.2015.117
9. Sun Z, Lei H, Zhang Z. Pre-B cell colony enhancing factor (PBEF), a cytokine with multiple physiological functions. Cytokine Growth Factor Rev 2013;24:433–42. 10.1016/j.cytogfr.2013.05.006
10. Samal B, Sun Y, Stearns G, et al. Cloning and characterization of the cDNA Encoding a novel human pre-B-cell colony-enhancing factor. Mol Cell Biol 1994;14:1431–7. 10.1128/mcb.14.2.1431-1437.1994
11. Revollo JR, Körner A, Mills KF, et al. Nampt/PBEF/Visfatin regulates insulin secretion in beta cells as a systemic NAD Biosynthetic enzyme. Cell Metabolism 2007;6:363–75. 10.1016/j.cmet.2007.09.003
12. Dalamaga M, Christodoulatos GS, Mantzoros CS. The role of extracellular and intracellular Nicotinamide Phosphoribosyl-transferase in cancer: diagnostic and therapeutic perspectives and challenges. Metabolism 2018;82:72–87. 10.1016/j.metabol.2018.01.001
13. Sun BL, Sun X, Casanova N, et al. Role of secreted extracellular Nicotinamide Phosphoribosyltransferase (eNAMPT) in prostate cancer progression: novel biomarker and therapeutic target. EBioMedicine 2020;61:103059. 10.1016/j.ebiom.2020.103059
14. Moschen AR, Kaser A, Enrich B, et al. Visfatin, an Adipocytokine with proinflammatory and Immunomodulating properties. J Immunol 2007;178:1748–58. 10.4049/jimmunol.178.3.1748
15. Colombo G, Clemente N, Zito A, et al. Neutralization of extracellular NAMPT (Nicotinamide Phosphoribosyltransferase) ameliorates experimental murine colitis. J Mol Med 2020;98:595–612. 10.1007/s00109-020-01892-0
16. Colombo G, Travelli C, Porta C, et al. Extracellular Nicotinamide Phosphoribosyltransferase BOOSTS IFNγ-induced macrophage polarization independently of Tlr4. iScience 2022;25:104147. 10.1016/j.isci.2022.104147
17. Audrito V, Serra S, Brusa D, et al. Extracellular Nicotinamide Phosphoribosyltransferase (NAMPT) promotes M2 macrophage polarization in chronic lymphocytic leukemia. Blood 2015;125:111–23. 10.1182/blood-2014-07-589069

18. Camp SM, Ceco E, Evenoski CL, et al. Unique toll-like receptor 4 activation by NAMPT/PBEF induces NFκB signaling and inflammatory lung injury. Sci Rep 2015;5:13135. 10.1038/srep13135
19. Van den Bergh R, Morin S, Sass HJ, et al. Monocytes contribute to differential immune pressure on R5 versus X4 HIV through the Adipocytokine Visfatin/NAMPT. PLoS ONE 2012;7:e35074. 10.1371/journal.pone.0035074
20. Torretta S, Colombo G, Travelli C, et al. The cytokine Nicotinamide Phosphoribosyltransferase (eNAMPT; PBEF; Visfatin) acts as a natural antagonist of C-C Chemokine receptor type 5 (Ccr5). Cells 2020;9:496. 10.3390/cells9020496
21. Managò A, Audrito V, Mazzola F, et al. Extracellular Nicotinate Phosphoribosyltransferase binds toll like receptor 4 And mediates inflammation. Nat Commun 2019;10:4116. 10.1038/s41467-019-12055-2
22. Ghaneialvar H, Shiri S, Kenarkoohi A, et al. Comparison of Visfatin levels in patients with breast cancer and endometrial cancer with healthy individuals: A systematic review and Meta-Analysis. Health Sci Rep 2022;5:e895. 10.1002/hsr2.895
23. Assiri AMA, Kamel HFM. Evaluation of diagnostic and predictive value of serum Adipokines: Leptin, Resistin and Visfatin in postmenopausal breast cancer. Obes Res Clin Pract 2016;10:442–53. 10.1016/j.orcp.2015.08.017
24. Zhu Y, Guo M, Zhang L, et al. Biomarker triplet NAMPT/VEGF/Her2 as a de novo detection panel for the diagnosis and prognosis of human breast cancer. Oncol Rep 2016;35:454–62. 10.3892/or.2015.4391
25. Kilkenny C, Browne WJ, Cuthill IC, et al. Improving Bioscience research reporting: the ARRIVE guidelines for reporting animal research. PLOS Biol 2010;8:e1000412. 10.1371/journal.pbio.1000412
26. Bellenghi M, Talarico G, Botti L, et al. Scd5-dependent inhibition of SPARC secretion hampers metastatic spreading and favors host immunity in a TNBC murine model. Oncogene 2022;41:4055–65. 10.1038/s41388-022-02401-y
27. Revell AD, Wang D, Boyd MA, et al. The development of an expert system to predict virological response to HIV therapy as part of an online treatment support tool. AIDS 2011;25:1855–63. 10.1097/QAD.0b013e328349a9c2
28. Zambelli F, Pesole G, Pavesi G. Pscan: finding over-represented transcription factor binding site motifs in sequences from Co-regulated or Co-expressed genes. Nucleic Acids Res 2009;37:W247–52. 10.1093/nar/gkp464
29. Courau T, Bonnereau J, Chicoteau J, et al. Cocultures of human colorectal tumor Spheroids with immune cells reveal the therapeutic potential of MICA/B and Nkg2A targeting for cancer treatment. J Immunother Cancer 2019;7:74. 10.1186/s40425-019-0553-9
30. Quijada H, Bermudez T, Kempf CL, et al. Endothelial eNAMPT Amplifies pre-clinical acute lung injury: efficacy of an eNAMPT-Neutralising Monoclonal antibody. Eur Respir J 2021;57:2002536. 10.1183/13993003.02536-2020
31. Sun BL, Tang L, Sun X, et al. A Humanized Monoclonal antibody targeting extracellular Nicotinamide Phosphoribosyltransferase prevents aggressive prostate cancer progression. Pharmaceuticals (Basel) 2021;14:1322. 10.3390/ph14121322
32. Grolla AA, Miggiano R, Di Marino D, et al. A Nicotinamide Phosphoribosyltransferase-GAPDH interaction sustains the stress-induced NMN/NAD^+ salvage pathway in the nucleus. J Biol Chem 2020;295:3635–51. 10.1074/jbc.RA119.010571
33. Gianchecchi E, Fierabracci A. Inhibitory receptors and pathways of lymphocytes: the role of PD-1 in Treg development and their involvement in Autoimmunity Onset and cancer progression. Front Immunol 2018;9:2374. 10.3389/fimmu.2018.02374
34. Armandi A, Colombo G, Rosso C, et al. The predictive role of extracellular NAPRT for the detection of advanced fibrosis in biopsy-proven non-alcoholic fatty liver disease. Int J Mol Sci 2023;24:1172. 10.3390/ijms24021172
35. Grolla AA, Travelli C, Genazzani AA, et al. Extracellular Nicotinamide Phosphoribosyltransferase, a new cancer Metabokine. Br J Pharmacol 2016;173:2182–94. 10.1111/bph.13505
36. Colombo G, Caviglia GP, Ravera A, et al. NAMPT and NAPRT serum levels predict response to anti-TNF therapy in inflammatory bowel disease. Front Med (Lausanne) 2023;10:1116862. 10.3389/fmed.2023.1116862
37. Wang Y, Wang F, Wang L, et al. NAD+ supplement potentiates tumor-killing function by rescuing

defective TUB-mediated NAMPT transcription in tumor-infiltrated T cells. Cell Reports 2021;36:109516. 10.1016/j.celrep.2021.109516

38. Barba C, Ekiz HA, Tang WW, et al. Interferon gamma-inducible NAMPT in Melanoma cells serves as a mechanism of resistance to enhance tumor growth. Cancers (Basel) 2023;15:1411. 10.3390/cancers15051411
39. Yoshida M, Satoh A, Lin JB, et al. Extracellular Vesicle-contained eNAMPT delays aging and extends LifeSpan in mice. Cell Metab 2019;30:329–42. 10.1016/j.cmet.2019.05.015
40. Patel ST, Mistry T, Brown JEP, et al. A novel role for the Adipokine Visfatin/pre-B cell colony-enhancing factor 1 in prostate carcinogenesis. Peptides 2010;31:51–7. 10.1016/j.peptides.2009.10.001
41. Buldak RJ, Gowarzewski M, Buldak L, et al. Viability and oxidative response of human colorectal HCT-116 cancer cells treated with Visfatin/eNampt in vitro. J Physiol Pharmacol 2015;66:557–66.
42. Park H-J, Kim S-R, Kim SS, et al. Visfatin promotes cell and tumor growth by Upregulating Notch1 in breast cancer. Oncotarget 2014;5:5087–99. 10.18632/oncotarget.2086
43. Gholinejad Z, Kheiripour N, Nourbakhsh M, et al. Extracellular NAMPT/Visfatin induces proliferation through Erk1/2 and AKT and inhibits apoptosis in breast cancer cells. Peptides 2017;92:9–15. 10.1016/j.peptides.2017.04.007
44. Soncini D, Caffa I, Zoppoli G, et al. Nicotinamide Phosphoribosyltransferase promotes epithelial-to-Mesenchymal transition as a soluble factor independent of its enzymatic activity. J Biol Chem 2014;289:34189–204. 10.1074/jbc.M114.594721
45. Cheng G, Liu C, Sun X, et al. Visfatin promotes Osteosarcoma cell migration and invasion via induction of epithelial-Mesenchymal transition. Oncol Rep 2015;34:987–94. 10.3892/or.2015.4053
46. Pylaeva E, Harati MD, Spyra I, et al. NAMPT signaling is critical for the Proangiogenic activity of tumor-associated neutrophils. Int J Cancer 2019;144:136–49. 10.1002/ijc.31808
47. Lv H, Lv G, Chen C, et al. NAD^+ metabolism maintains inducible PD-L1 expression to drive tumor immune evasion. Cell Metab 2021;33:110–27. 10.1016/j.cmet.2020.10.021
48. Ahn E, Araki K, Hashimoto M, et al. Role of PD-1 during Effector Cd8 T cell differentiation. Proc Natl Acad Sci U S A 2018;115:4749–54. 10.1073/pnas.1718217115